

Omnidirectional and independently tunable defect modes in fractal photonic crystals containing single-negative materials

Y.H. Chen

Received: 28 October 2008 / Revised version: 27 February 2009 / Published online: 3 April 2009
© Springer-Verlag 2009

Abstract The properties and applications of omnidirectional and independently tunable defect modes in fractal photonic crystals containing single-negative materials are demonstrated. The proposed fractal structures can produce as many defect modes as desired by adjusting its structural parameters. The interaction effect between the defect states of such fractal structures is avoided, so the frequency of each defect mode can be tuned independently. Furthermore, these defect modes inside the zero effective-phase gap are insensitive to the incident angle. With perfect transmission, mode controllability and omnidirectional compatibility, these structures open a promising way for designing omnidirectional multichannel filters with specific channels.

PACS 42.70.Qs · 41.20.Jb · 78.20.Ci

1 Introduction

Experimental and theoretical studies of artificially manufactured periodic dielectric media called photonic band gap (PBG) materials or photonic crystals (PCs) have attracted considerable attention in recent years [1, 2]. The PC structures inhibit the propagation of electromagnetic waves in a certain range of frequencies, in analogy with electronic band gaps in semiconductors. By breaking the periodicity of the PC, it is possible to create highly localized defect

modes within the PBG, leading to the phenomenon of multiple channeled filtering [3, 4]. A multichannel filter based on one-dimensional (1D) PC is one of the important components widely used in communication and electro-optical systems [5–7]. However, in conventional PC structures consisting of positive-index materials (PIMs), the defect modes of the PC are interactional and thus cannot be tuned independently. This will increase the difficulty for the design of multichannel filter with specific channels. Moreover, the resonant frequencies of the defect modes will shift to higher frequencies as the incident angle increases. This makes the filters inefficient in situations of multidirectional incidence. So the applications of the multichannel filters are restricted.

Recently, metamaterials, in which only one of the material parameters has a negative value, have been realized [8, 9]. These single-negative (SNG) materials include the mu-negative (MNG) media with negative permeability μ but positive permittivity ϵ and epsilon-negative (ENG) media with negative ϵ but positive μ . It is found that stacking alternating layers of MNG and ENG media leads to a type of PBG corresponding to a zero effective phase (φ_{eff}) [10]. When SNG defect layers are introduced, a pair of defect modes is found in this gap [11, 12]. Moreover, multiple omnidirectional resonance modes can also be generated in photonic heterostructures containing SNG materials [13–15]. These defect modes or resonance modes in the zero- φ_{eff} gap show weak dependence on the incident angle. In this paper, fractal 1D PCs containing single-negative materials are proposed. We demonstrate that the frequency of each defect mode of such PC structures can be tuned separately and is insensitive to the incident angle. Such properties will lead to potential applications.

Y.H. Chen (✉)
School of Physics and Telecommunication Engineering,
South China Normal University, Guangzhou 510006,
China
e-mail: kallenmail@sina.com
Fax: +86-20-39310882

2 Computational model and numerical method

There are two main approaches to realize single-negative (SNG) materials that have been reported: resonant structures made of a periodic array of metallic wires [8] or split-ring resonators [9] and nonresonant transmission line structures made of inductors and capacitors [16–18]. The former can be utilized in three-dimensional space and high frequencies, but they have relatively high losses and a narrow bandwidth. The latter shows advantages of lower loss and wider bandwidth and has already been implemented in various component and microwave applications. According to the equivalent transmission lines models [16], MNG material can be viewed as distributed series and shunt capacitors, while ENG material can be viewed as distributed series and shunt inductors. The SNG materials have Drude dispersion when they are realized by the distributed L–C transmission lines [19, 20]. In the following calculation, we use Drude models to describe the single-negative materials, that is,

$$\varepsilon_1 = \varepsilon_a, \quad \mu_1 = \mu_a - \frac{\omega_{\text{mp}}^2}{\omega^2} \quad (1)$$

in MNG materials and

$$\varepsilon_2 = \varepsilon_b - \frac{\omega_{\text{ep}}^2}{\omega^2}, \quad \mu_2 = \mu_b \quad (2)$$

in ENG materials. In (1) and (2), ω_{mp} and ω_{ep} are the magnetic plasma frequency and the electronic plasma frequency, respectively. The frequency $v (= \omega/2\pi)$ is in units of gigahertz. In our calculation, the material parameters are selected as $\mu_a = \varepsilon_b = 1$, $\varepsilon_a = \mu_b = 3$ and $\omega_{\text{mp}} = \omega_{\text{ep}} = 10$ GHz. The construction procedure of 1D fractal photonic structure is based on the method of coupling defect layers. Begin with a periodic multilayer initiator S_0 of $(N_\mu N_\varepsilon)^m$ or $(N_\varepsilon N_\mu)^m$. N_μ and N_ε represent the layers of MNG and ENG materials, respectively, with the thickness of d_{N_μ} and d_{N_ε} . m is the number of periods. Then, by coupling a defect layer between the initiators $(N_\mu N_\varepsilon)^m$ and $(N_\varepsilon N_\mu)^m$ one forms the first stage of the fractal $S_1 = (N_\mu N_\varepsilon)^m D_1 (N_\varepsilon N_\mu)^m$. Next, when another defect layer is inserted between two structures of S_1 , the second stage of fractal S_2 is formed. It is possible to obtain a self-similar fractal structure by repeating the given operation. The lower-order fractal sequences are given by

$$\begin{aligned} S_0 & (N_\mu N_\varepsilon)^m \\ S_1 & (N_\mu N_\varepsilon)^m D_1 (N_\varepsilon N_\mu)^m \\ S_2 & (N_\mu N_\varepsilon)^m D_1 (N_\varepsilon N_\mu)^m D_2 (N_\mu N_\varepsilon)^m D_1 (N_\varepsilon N_\mu)^m \\ S_3 & (N_\mu N_\varepsilon)^m D_1 (N_\varepsilon N_\mu)^m D_2 (N_\mu N_\varepsilon)^m D_1 (N_\varepsilon N_\mu)^m \\ & \times D_3 (N_\mu N_\varepsilon)^m D_1 (N_\varepsilon N_\mu)^m D_2 (N_\mu N_\varepsilon)^m D_1 (N_\varepsilon N_\mu)^m \\ \vdots & \end{aligned}$$

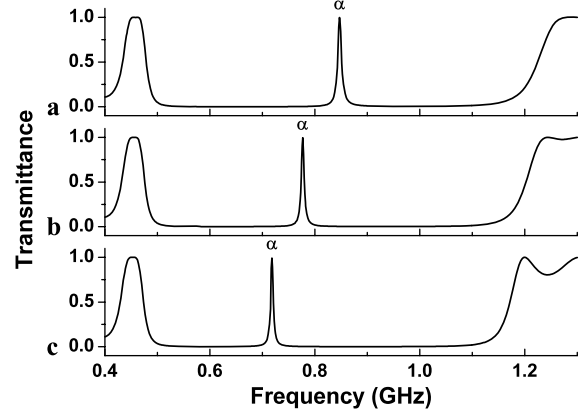


Fig. 1 Transmission spectra of the fractal structure $S_1 = (N_\mu N_\varepsilon)^8 \times D_1 (N_\varepsilon N_\mu)^8$ with (a) $d_1 = 40$ mm, (b) $d_1 = 50$ mm, and (c) $d_1 = 60$ mm

D_1 , D_2 and D_3 are PIM defect layers with the thicknesses of d_1 , d_2 and d_3 , respectively. Here we choose $d_{N_\mu} = 6$ mm, $d_{N_\varepsilon} = 10$ mm, and $\varepsilon_{D_i} = \mu_{D_i} = 2.0$, ($i = 1, 2, 3$).

Let a wave be incident at an angle θ from vacuum onto the considered fractal structure. Suppose that the wave in the l th layer has a wave vector $\mathbf{k}_l = k_{lx}\hat{x} + k_{lz}\hat{z}$, whose magnitude is $\omega n_l/c$ (where c is the speed of light in vacuum). The amplitudes of the forward and the backward wave of the electric component can be related via a transfer matrix

$$M_l = \begin{pmatrix} \cos k_{lz}d_1 & i \sin k_{lz}d_1/\eta_l \\ i\eta_l \sin k_{lz}d_1 & \cos k_{lz}d_1 \end{pmatrix}, \quad (3)$$

where $\eta_l = \eta_l^s = ck_{lz}/\omega\mu_l$ for TE wave, and $\eta_l = \eta_l^p = \omega\varepsilon_l/c k_{lz}$ for TM wave. The transmittance and field distributions of the structure can be obtained by means of the transfer-matrix method.

3 Omnidirectional and independently tunable defect modes

The initiator S_0 is a periodic structure, where a zero- φ_{eff} gap originating from a tunneling mechanism exists [10]. The first stage of fractal S_1 is a 1D PC with a defect layer, where a defect mode will appear in the zero- φ_{eff} gap. Figure 1 shows the transmittance of the fractal structure $S_1 = (N_\mu N_\varepsilon)^8 D_1 (N_\varepsilon N_\mu)^8$ at normal incidence. As shown in Fig. 1, the zero- φ_{eff} gap exists in the frequency range from about 0.5 to 1.1 GHz, and the frequency of defect mode α can be tuned by changing the thickness d_1 .

Next, we consider the second stage of fractal S_2 . Figure 2 gives the transmission spectra of $S_2 = (N_\mu N_\varepsilon)^8 D_1 (N_\varepsilon N_\mu)^8 \times (N_\varepsilon N_\mu)^8 D_2 (N_\mu N_\varepsilon)^8 D_1 (N_\varepsilon N_\mu)^8$ at normal incidence. As shown in Fig. 2, another defect mode β appears. In Fig. 2(a), we fix $d_1 = 60$ mm and increase d_2 from 20 to 25 to 30 mm. It can be seen that defect mode α remains nearly

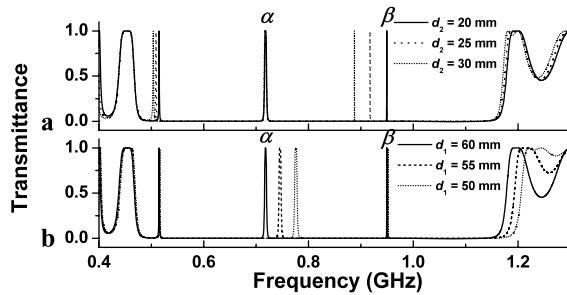


Fig. 2 Transmission spectra of the fractal structure $S_2 = (N_\mu N_\epsilon)^8 \times D_1(N_\epsilon N_\mu)^8 D_2(N_\mu N_\epsilon)^8 D_1(N_\epsilon N_\mu)^8$ with (a) $d_1 = 60$ mm and $d_2 = 20, 25, 30$ mm, (b) $d_2 = 20$ mm and $d_1 = 60, 55, 50$ mm

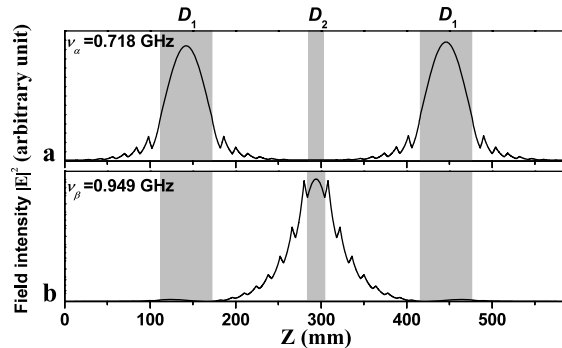


Fig. 3 Electric field distributions corresponding to the two defect modes (a) α and (b) β of S_2 in Fig. 2 with $d_1 = 60$ mm and $d_2 = 20$ mm. The light gray areas correspond to the PIM defect layers

invariant, while defect mode β shifts from 0.949 to 0.917 to 0.886 GHz. Similarly, defect mode β is stable, while defect mode α shifts from 0.718 to 0.775 GHz when keeping d_2 unvaried and changing d_1 from 60 to 50 mm, as shown in Fig. 2(b). Thus, the frequency of defect mode α or β can be tuned independently in a large range without affecting the other defect mode. It means that the interaction effect between the two defect modes of the proposed structure is avoided. To show how the defect modes are generated in the zero- φ_{eff} gap case, the electric field distributions inside the fractal structures are investigated at frequencies of defect modes α and β , as shown in Fig. 3. It is seen in Fig. 3(a) that the electric field corresponding to defect mode α is strongly localized in both defect layers D_1 but not in defect layer D_2 . On the other hand, the electric field corresponding to defect mode β is mainly localized in D_2 but not in D_1 , as shown in Fig. 3(b). Therefore, the coupling layers of D_1 and D_2 are two different kinds of defects and respectively relate to corresponding defect states. The wave functions of the two kinds of defect states do not overlap and their bases are orthogonal, leading to the independency among the defect modes.

Then we investigate the third stage, of fractal S_3 . Figure 4 gives the transmission spectra of S_3 with $m = 8$ for different d_1, d_2 and d_3 , respectively. A new defect mode γ

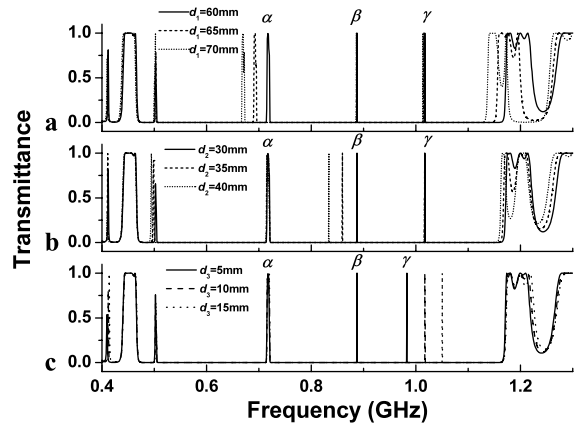


Fig. 4 Transmission spectra of the fractal structure $S_3 = (N_\mu N_\epsilon)^8 D_1(N_\epsilon N_\mu)^8 D_2(N_\mu N_\epsilon)^8 D_1(N_\epsilon N_\mu)^8 D_3(N_\mu N_\epsilon)^8 D_1(N_\epsilon N_\mu)^8 \times D_2(N_\mu N_\epsilon)^8 D_1(N_\epsilon N_\mu)^8$ with (a) $d_2 = 30$ mm, $d_3 = 10$ mm and $d_1 = 60, 65, 70$ mm, (b) $d_1 = 60$ mm, $d_3 = 10$ mm and $d_2 = 30, 35, 40$ mm, (c) $d_1 = 60$ mm, $d_2 = 30$ mm and $d_3 = 5, 10, 15$ mm

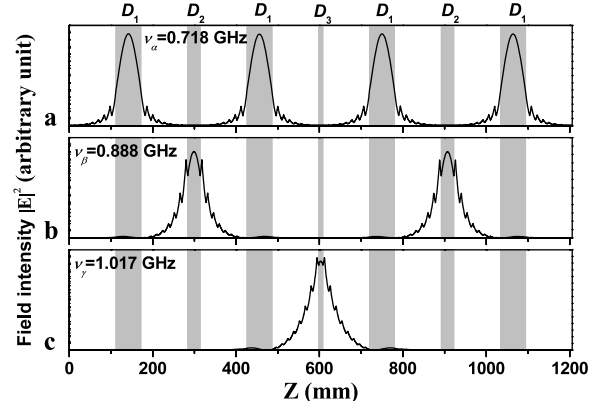


Fig. 5 Electric field distributions corresponding to the three defect modes of S_3 in Fig. 4 with $d_1 = 60$ mm, $d_2 = 30$ mm, and $d_3 = 10$ mm. The light gray areas correspond to the PIM defect layers

has been produced. It can be seen that all of the three defect modes can be tuned independently. If defect mode α needs to be moved to a definite frequency while keeping β and γ fixed, one only needs to adjust d_1 to match the demand, and the same to the defect mode β or γ . In Fig. 5 we calculate the electric field distributions corresponding to the three defect modes of the structure S_3 . It is seen that the electric field of the defect mode α , β , and γ are strongly localized in D_1 , D_2 , and D_3 , respectively. The three defect modes relate to three different kinds of defect states respectively; therefore, their frequencies can be independently adjusted. According to the fractal rule, PCs with more than three independently tunable defect modes can also be designed.

In the above discussion, the incident wave is assumed to be normal. It is known that conventional multichannel fil-

Fig. 6 Transmittance vs. incident angles and frequencies of the structure $S_1 = (N_\mu N_\varepsilon)^8 \times D_1(N_\varepsilon N_\mu)^8$ with $d_1 = 40$ mm

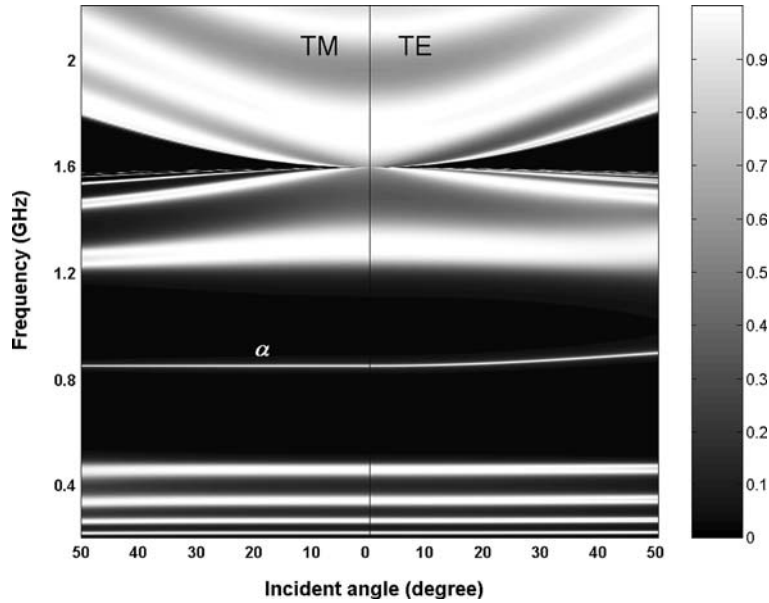
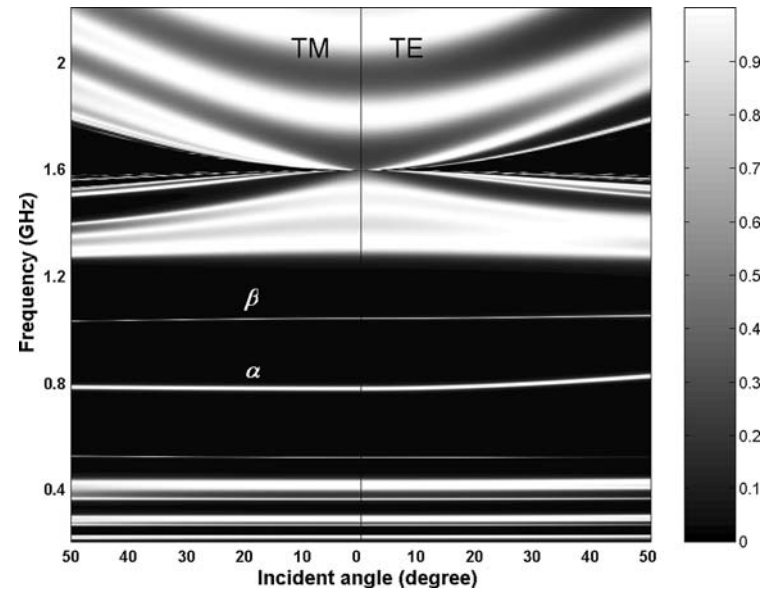


Fig. 7 Transmittance vs. incident angles and frequencies of the structure $S_2 = (N_\mu N_\varepsilon)^8 \times D_1(N_\varepsilon N_\mu)^8 D_2(N_\mu N_\varepsilon)^8 D_1(N_\varepsilon N_\mu)^8$ with $d_1 = 50$ mm and $d_2 = 10$ mm



ters are sensitive to the incident angle, making them inefficient for applications in the case of multidirectional incidence. Next, we turn to investigation of the dependence of the defect modes on the incident angle in our fractal structures containing SNG materials. Figure 6 gives the transmittance of S_1 for different incident angles and polarizations with $d_1 = 40$ mm. As shown in Fig. 6, as the incident angle changes, defect mode α shifts very slowly. Similarly, it can be seen from Fig. 7 that both defect modes α and β of structure S_2 are insensitive to the incident angle. Particularly, the frequency of β is almost unchanged as the incident angle varies. Therefore, our fractal PC structures are very useful for the design of multichannel filters with specific channels and a large incident angle.

4 Conclusion

In conclusion, fractal PCs containing SNG materials are proposed and investigated. The fractal structure can generate multiple defect modes, their number can be controlled by adjusting the structural parameters. The frequencies of these defect modes inside the zero- φ_{eff} gap can be independently tuned and are insensitive to the incident angle. Hence, such fractal structures provide an easy way to select useful multichannel optical signals from a stop gap, and it is useful in optical device applications.

Acknowledgements This work is supported by the National Natural Science Foundation of China (Grant No. 10704027), and the Natural Science Foundation of Guangdong Province of China (Grant No. 07300205).

References

1. E. Yablonovitch, Phys. Rev. Lett. **58**, 2059 (1987)
2. S. John, Phys. Rev. Lett. **58**, 2486 (1987)
3. E. Yablonovitch, T.J. Gmitter, R.D. Meade, A.M. Rappe, K.D. Brommer, J.D. Joannopoulos, Phys. Rev. Lett. **67**, 3380 (1991)
4. S. Noda, A. Chutinan, M. Imada, Nature **407**, 608 (2000)
5. Q. Qin, H. Lu, S.N. Zhu, C.S. Yuan, Y.Y. Zhu, N.B. Ming, Appl. Phys. Lett. **82**, 4654 (2003)
6. Z.S. Wang, L. Wang, Y.G. Wu, L.Y. Chen, X.S. Chen, W. Lu, Appl. Phys. Lett. **84**, 1629–1631 (2004)
7. S.W. Wang, C. Xia, X. Chen, W. Lu, M. Li, H. Wang, W. Zheng, T. Zhang, Opt. Lett. **32**, 632 (2007)
8. J.B. Pendry, A.J. Holden, W.J. Stewart, I. Youngs, Phys. Rev. Lett. **76**, 4773 (1996)
9. J.B. Pendry, A.J. Holden, D.J. Robbins, W.J. Stewart, IEEE Trans. Microw. Theory Tech. **47**, 2075 (1999)
10. H.T. Jiang, H. Chen, H.Q. Li, Y.W. Zhang, J. Zi, S.Y. Zhu, Phys. Rev. E **69**, 066607 (2004)
11. Y.H. Chen, J.W. Dong, H.Z. Wang, Appl. Phys. Lett. **89**, 141101 (2006)
12. Y.H. Chen, Appl. Phys. Lett. **92**, 011925 (2008)
13. Y.H. Chen, J.W. Dong, H.Z. Wang, J. Opt. Soc. Am. B **23**, 2237 (2006)
14. Y.J. Xiang, X.Y. Dai, S.C. Wen, D.Y. Fan, J. Opt. Soc. Am. A **24**, A28 (2006)
15. Y.H. Chen, J. Opt. Soc. Am. B **25**, 1794 (2008)
16. A. Alù, N. Engheta, IEEE Trans. Antennas Propag. **51**, 2558 (2003)
17. T. Fujishige, C. Caloz, T. Itoh, Microw. Opt. Technol. Lett. **46**, 476 (2005)
18. H.Y. Li, Y.W. Zhang, L.W. Zhang, L. He, H.Q. Li, H. Chen, J. Appl. Phys. **102**, 033711 (2007)
19. G.V. Eleftheriades, A.K. Iyer, P.C. Kremer, IEEE Trans. Microw. Theory Tech. **50**, 2702 (2002)
20. L.W. Zhang, Y.W. Zhang, L. He, H.Q. Li, H. Chen, Phys. Rev. E **74**, 056615 (2006)